Int. J. Electrochem. Sci., 12 **(2017)** 6638 – 6652, doi: 10.20964/2017.07.31

International Journal of ELECTROCHEMICAL SCIENCE
www.electrochemsci.org

Enhanced Interfacial Properties of Electrochemically Deposited ZnO Nano Structured Electrode

K. Selvarani. K[1], *ShamimaHussain*[2], *R. Prasanth*[1,*]

[1] UNESCOMadanjeet School of Green Energy Technology, Pondicherry University
[2] UGC - DAE Consortium for Scientific Research, Pondicherry, India, 605014.
[*]E-mail: prasanth.get@pondiuni.edu.in

Received: 13 March 2017 / *Accepted:* 30 April 2017 / *Published:* 12 June 2017

The electronic properties at the transparent conducting oxide (TCO)/ semiconductor interface are crucial in optimizing the efficiency of light harvesting and storage devices. The back scattered current and surface defects of ZnO nanorods at interface limit the commercial level fabrication of device structures with this material system. Herein, a cost effective and scalable electro-nanofabrication technique has been utilized for the growth of ZnO nanorods over seeded TCO substrates. The electrochemical conditions for controlling ZnO nano rod morphology over the ZnO self-seeded transparent conducting oxide coated glass substrate are comprehensively investigated. The results show that the seed layer thickness, annealing environment for seeding and growth as well as processing temperatures are critical in optimizing the electronic properties at the interface. By controlling these parameters the back scattering current has been reduced to record minimum of 10^{-7} A and the interfacial resistance has been minimized to 30 Ω. Photoluminescence spectroscopy and the Electrochemical Impedance spectroscopy are effectively used in this study for defect center analysis and interfacial characterization.

Keywords: ZnO nanorods, Electro deposition, interfacial resistance, back scattering current

1. INTRODUCTION

Research in one dimensional nanostructures gathered momentum in recent years because of its unique properties that are valuable for electronic, magnetic, optical and photo catalytic applications [1, 2]. ZnO is a prominent “green” material for fabricating one dimensional nanostructure array electrodes for achieving high carrier mobility in solar cells [3], fuel cells [4], bio sensors [5], gas sensors [6] etc. The wide band gap (3.37 eV) with high exciton binding energy (60 eV) at room temperature makes it a potential candidate for electrodes in device structure. The piezo and pyro electric properties of ZnO nanorods are useful for nano generators [7], transducers [8], sensors etc. We also demonstrated polariton confinement [9] and resonance enhancement [10] in ZnO nanorods that

leads to polariton lasers [11]. However, the interfacial resistance, charge recombination processes due to the existence of different defect centres play major role in the efficiency of electrical and optoelectronic devices with ZnO nanostructures.

ZnO nanorods are widely synthesized by high temperature (500-900^0 C) physical vapor deposition [12], VLS method [10] or sol gel technique [13]. These techniques are generally expensive, slow and difficult to grow over flexible substrates. The hydro thermal method [14] is simple and cost effective. However, it generally needs high temperature around 200 ^{0}C and long growth time (4 hrs to 5 days). Control over the growth parameters such as orientation, rod number density, rod dimensions are difficult to achieve.

Many sincere efforts have been made by researchers to make high quality ZnO thin films and nano wire arrays by electrochemical approach [15- 16]. However, because of the high sensitivity of morphology over wide range of electrochemical growth parameters a systematic investigation on the dependence of growth parameters, especially growth temperature is required in order to make the growth possible over flexible substrate. The goal of the present investigation is to understand the optimum electrochemical conditions for the vertically oriented growth of ZnO nanorods over TCO coated substrates. ZnO seed layer is used to achieve vertically oriented rod array [17]. Even though the seed free growth can provide limited verticality [18], the growth control and the optimization of interfacial resistance of the TCO and the rod layer are difficult to achieve with seedless growth. In this two-step process reported here seeding is done with a pulse electro chemical deposition (P-ECD) and the nanostructure growth is carried out in continuous Electro Chemical Deposition (ECD). As ECD has multiple growth parameters for the control of nanorod morphology compared to hydrothermal technique. For both seed and nanostructure growth the solution concentration, applied potential and current density are same in this report. Both steps are done with 73^{0}C and with a growth rate of 0.5nm/sec. The electrochemical parameters such as applied potential, current density, concentration of the precursor, supporting electrolyte, Oxygen flow rate, temperature and the P^H are used to control the number density of rods, rod diameter, length and orientation of rods. The nanorod diameter is increased by increasing the charge density and temperature in turn the solubility of Zn $(OH)^{-2}$ which increases the availability of OH^- ion at the surface, during nucleation [19]. The increased P^H increases the solubility of the Zn $(OH)^{-2}$ species with temperature. The recombination reaction due to the surface defects is prominent in ZnO photo anodes [20, 21]. This will adversely affect the conversion efficiency of energy harvesting devices such as solar cell and fuel cells.

In this work the ZnO nanorod array electrode is synthesized by optimizing the conditions for electrochemical deposition and the defect center modification has been investigated in post annealing process in the presence of air, oxygen and nitrogen. The seed layer thickness is optimized for efficient charge collection at the conducting glass plate (FTO) by lowering the electron back scattering. The modification of the rod density in relation to the availability of the ionic availability at the growing surface of the nanostructure is studied by varying the Oxygen flow rate. The cathodic formation potentials of ZnOH and ZnO species are measured for different temperatures to find the lowest possible temperature for the ECD of ZnO. The modification in carrier density and flat band potential during the device fabrication (where the electrode undergoes thermal treatments) is also well understood through this study.

2. EXPERIMENTAL

Substrate Preparation: The FTO glass plates are cleaned with acetone and then ultra sonicated in acetone and in De- Ionized water (DI water) at 50 degrees for 20 minutes each. Then the plates are dried in N_2 stream and kept in desiccators for further use.

Electrochemical Conditions and precursor solution: The ECD and P-ECD has been done with the following precursor and electro chemical conditions. The precursor is 5mM of $ZnCl_2$ and 0.5M of KCl in DI water of 20 ml for seeding and 80 ml for ZnO nanorod synthesis respectively. The solution temperature is maintained at 73^{o}Cfor both seeding layer and rod growth. The cathodic potential applied to the working electrode is – 1.1V. A Pt mesh of (2.25 cm x 2.25cm) is used as a counter electrode and the Ag/AgCl is used as a reference electrode to maintain the potential constant during the deposition. Using ECD and P-ECD seed layers of thickness 40 nm, 60 nm, 80 nm, 100 nm and 120 nm has been coated by varying the deposition time.

Spin coating a 0.6M Zinc acetate in methoxyethanol and monoethanolamine solution is made and the spin coating is done for 2500 rpm. Seed layers of thickness 40 nm, 60 nm, 80 nm and 100 nm are coated and then sintered at 100 ^{o}C for 10 minutes.

Seeding: Three different techniques such as spin coating, ECD and P-ECD are investigated for the fabrication of seed layer in this study. Electrodes are prepared with multi-layers of seed. In all electrodes ZnO nanorod arrays are deposited over the seed layer with ECD technique. The results are analyzed with SEM images for desired morphology. Scanning electron monographs shows that the ZnO nanorod array over the P-ECD seeds has better vertical alignment, controllable rod number-density and diameter. So P-ECD method is opted for seed layer for further investigation. The P-ECD layers provide better nucleation centers for the vertically oriented growth of ZnO nanorods. The pulse timing is maintained as 100 sec for each layer of 20 nm thickness. For investigating the effect of thermal treatment the seed layer is annealed in Nitrogen, Oxygen atmosphere and air at 130^{o}C for 20 minutes and compared the results with un-annealed samples.

Nanorod array synthesis: The un-annealed and annealed seeded substrates are used for the nanorod array synthesis. The Amperometry for 2000 secs is done with the Metrohm Autolab 84344 Galvanostat potentiostat at a cathodic potential 0f -1.1V in controlled Oxygen bubbling with Alicat Scientific Mass flow controller MC 5SLPM-D with Flow vision MX. The synthesized nanorod array is cleaned with stream of DI water and dried in N_2 stream. The sample is maintained in desiccators for further characterization. The samples are annealed at 130 ^{0}C for 20 minutes at air, oxygen and nitrogen environment. Performances of the electrodes are compared with the un-annealed samples.

Characterization: The electrochemical conditions for seeding, rod growth and orientation of the rods have been optimized using the scanning electron monographs in Hitachi 3400 model. The Keithley 2400 with Labview interfacing environment is used for dark current measurement. Metrohm Autolab 84344 Galvanostat potentiostat with Nova is used for the cyclic voltammetry (CV) analysis. The Mott Schottky (MS) analysis and impedance studies are carried out in Autolab 84344. The Horiba jobin Yvon SPEX – F311 spectro - flourimeter is used for the PL analysis for the defect emission studies.

3. RESULTS AND DISCUSSION

The electrochemical fabrication of ZnO nanorod is carried out over ZnO seeded Fluorine doped Tin Oxide substrate. The seed layer improves the lattice matching of the substrate to the nanorod layer. Hence, better orientation of crystal plane alignment between the rod and the TCO can be obtained. The lattice matching due to seed-rod layer leads to the reduction of resistance at the interface.

The seed layers deposited with spin coating, ECD and P_ECD have thickness varies from 60 nm to 120 nm one from each are depicted as seed 1 as s1, seed 2 as s2 and seed 3 as s3 in Figure 1. Electrochemical depositions of ZnO nanorod layer has been carried out in all the seed samples and are depicted as rod sample on s1 as r1, rod sample on s2 as r2 and the rod sample on s3 as r3 in Figure 1. Scanning electron monographs show that there is no rod formation over the spin coated seed layer, as the ZnO particles are dispersed in random orientations and during the annealing the agglomeration happens in non-uniform sizes.

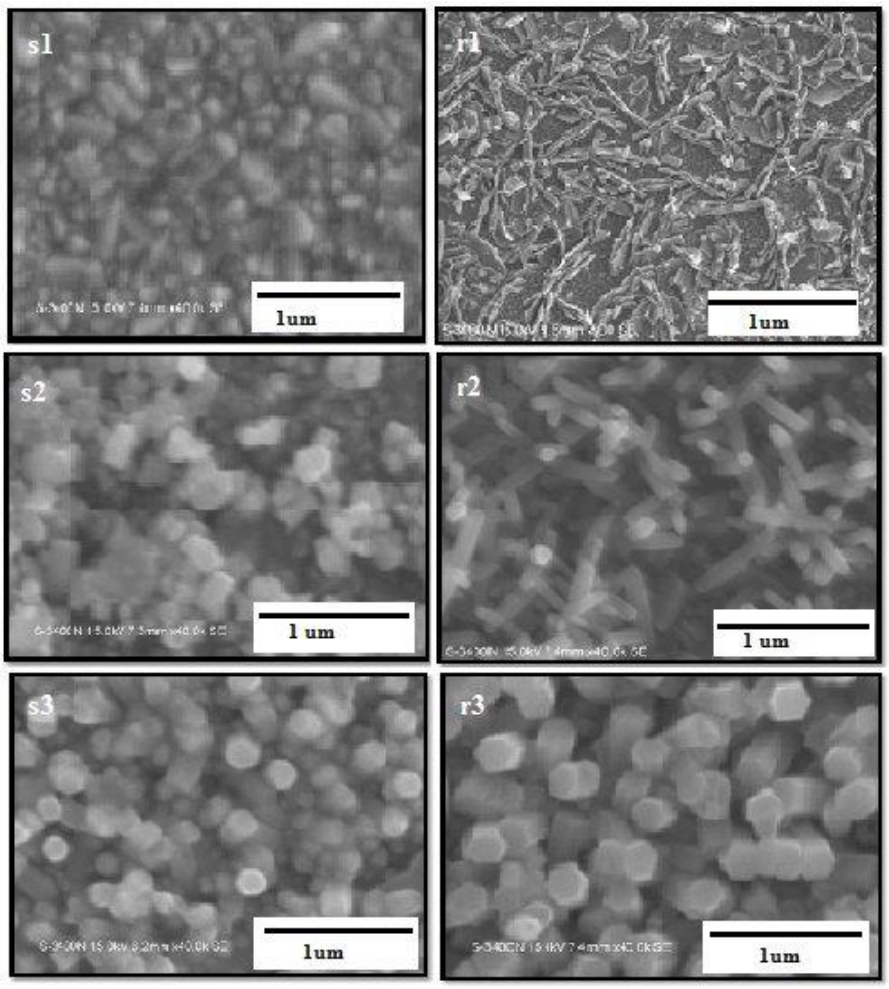

Figure 1. Scanning Electron Microscope images of s1, s2, s3, r1, r2, r3.

Over the ECD seed layer the nanorods are arranged in zigzag manner. During the seed layering the ZnO get continuously deposited at the nucleated sites in the direction of the availability of the Zn^{2+}

and the OH^-species. The lattice arrangement of the seeds in every point on the surface is in conformal with the sustained availability of Zn^+ and OH^- species at the rod growing face.

The nanorod layer grown over P-ECD seed shows more vertical alignment. In this method at every initiation of pulse, the charges are available at the tip of the surfaces. Hence, the growth happens only on the tip surface. This favors the spontaneous vertical C-axis growth of oriented ZnO rods in the second step ECD deposition.

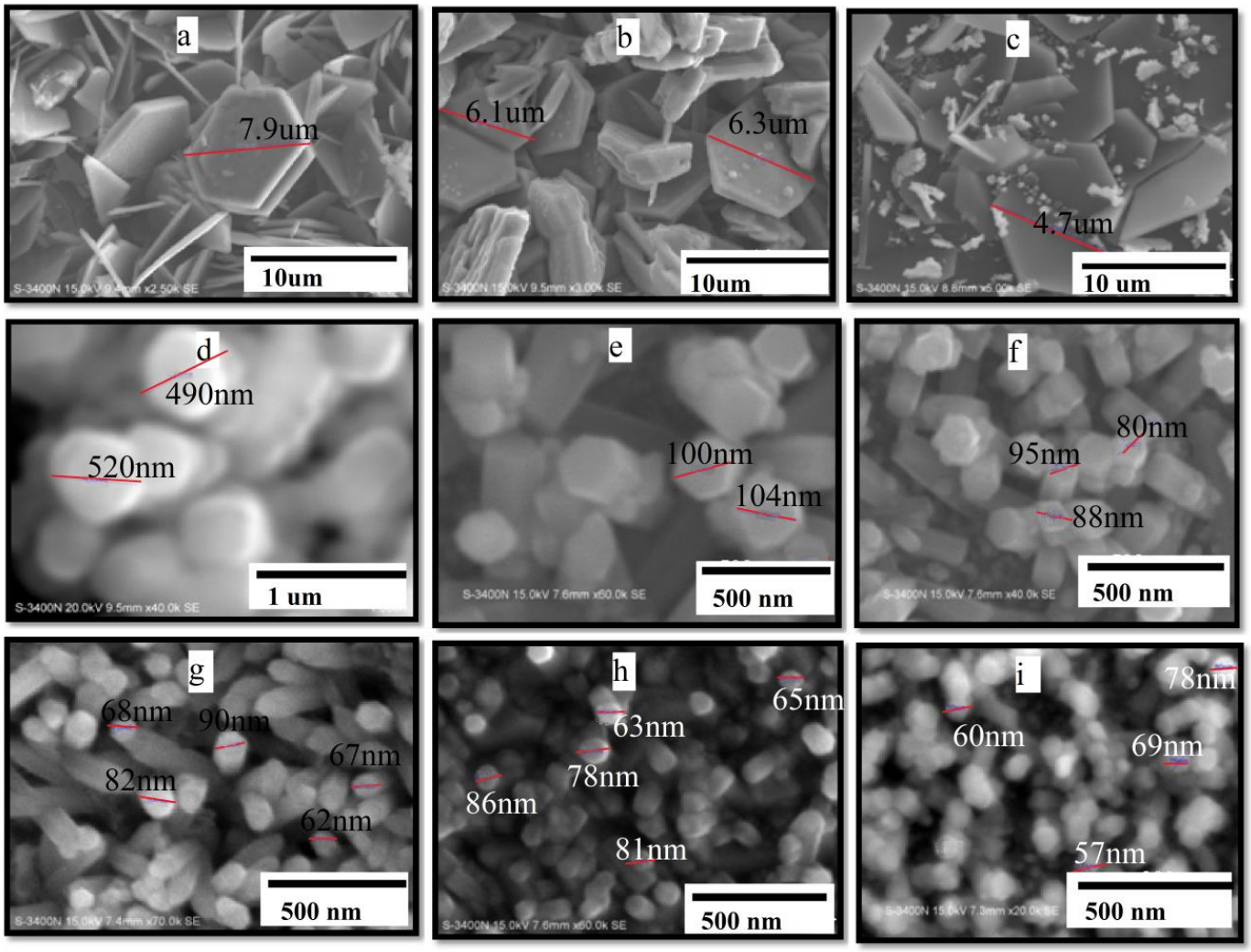

Figure 2. The effect of oxygen flow in the morphology of ECD ZnO nano rods grown over the P-ECD seed of 100 nm thickness.

Effect of Oxygen flow control: The effect of oxygen flow rate in controlling the radius of the nano rods is shown in figure (2), the images 'a,b,c,d,e,f,g, and h, i are the nanorods deposited with the Oxygen flow rates of 0.5,0.2,0.05,0.01,0.005,0.0025,0.001 and 0.0005 sccm. At the growth site the Zn is available from the precursor; the externally supplied oxygen flow rate can be used as one of the electrochemical nanofabrication control parameter for fixing the rod radius. The supply of Oxygen at 0.5 sccm only hexagonal ZnO flakes having diameter in micrometer range was formed. The oxygen

pressure is reduced below 0.05 sccm different diameter nanorods are formed. Variation of diameter with respect to the oxygen flow rate is illustrated in figure (3) (Formation of micron size structures at higher oxygen flow rate is given in the inset). The flow is maintained constant during the growth process to have the uniform diameter throughout the length of the rods. The reduced oxygen availablity at the non polar surfaces retards the lateral growth of ZnO rods. The surface energy of the alternate Zn- terminated and O- terminated polar planes of the ZnO structure should be larger than the non-polar planes for the vertical growth of the rods. The availability of the O- only at the polar surface and not on the lateral side gives the uniformity of the rod diameter throughout the length of the rods and its verticality. Table (1) gives the number density of the nanorods for different Oxygen flow rates. The Oxygen flow rate is controlled by the mass flow controller to vary the rod diameter in turn the rod density. As rod diameter increases the number of rods per unit area changes. The rod densities per unit micrometer area are measured with the ImageJ software on the SEM images of the samples with different Oxygen flow rates as in the table. The lengths of the rods are around 1.1 to 1.5μm leads to an average growth rate of 0.4nm/sec to 0.5nm /sec. Thus the regulated supply of oxygen facilitates the epitaxial staking layer growth kinetics favors the uniform rod morphology.

Table 1: Number density of nanorods for different oxygen flow rate.

Sl no	Oxygen flow(sccm)	Number density of rods/μm^2
1	0.5	1
2	0.2	3
3	0.05	4
4	0.01	12
5	0.005	28
6	0.0025	65
7	0.001	150
8	0.0005	180

Even though the ZnO can be deposited with an applied potential ranges between -0.8 V and -1.6V [22], formation rate of ZnO is maximum at -1.1V. The growth temperature is then optimized for this potential. The deposition is tried with different temperature and the lowest possible temperature is determined by finding the formation peaks for the nucleation of ZnO. The cyclic voltammogram of the deposition is recorded at different temperatures. The basic chemical reaction for the deposition is as follows [23],

$Zn^{2+} + 0.5O_2 \rightarrow 2e^- + ZnO$

$Zn^{2+} + H_2O + 0.5\ O_2 \rightarrow 2ZnOH + 2e^-$

Zinc is hydrolyzed in the presence of oxygen and then ZnOH is dehydrated to ZnO. The formation of ZnOH and ZnO species at different temperatures is analyzed with the cyclic voltammetry for a range of temperature varies from 35 ^{0}C to 75^{0}C, in 5 ^{o}C steps figure (4). The cathodic peak for the formation of ZnOH is observed between -0.3 V to -0.48 V which is a progressive process. The ZnO formation peak is obtained at -0.048 V which is an instantaneous process. The formation of ZnOH and

ZnO is predominantly seen only after 70 ^{0}C as in the voltammogram. Up to 70^{0}C all the Zn species is exhausted for the ZnOH formation and not available for the formation of ZnO. Below 70 ^{0}C there are no peaks for the ZnO has been observed. The dehydration of ZnOH to ZnO happens only after 70^{o}C. Hence, the lowest temperature of deposition for this optimized potential (-1.1 V) is 70 ^{0}C. (For all structures reported in this article we maintained the growth temperature at 73 ^{o} C). As the deposition temperature is below150^{0}C it is suitable even for flexible substrates.

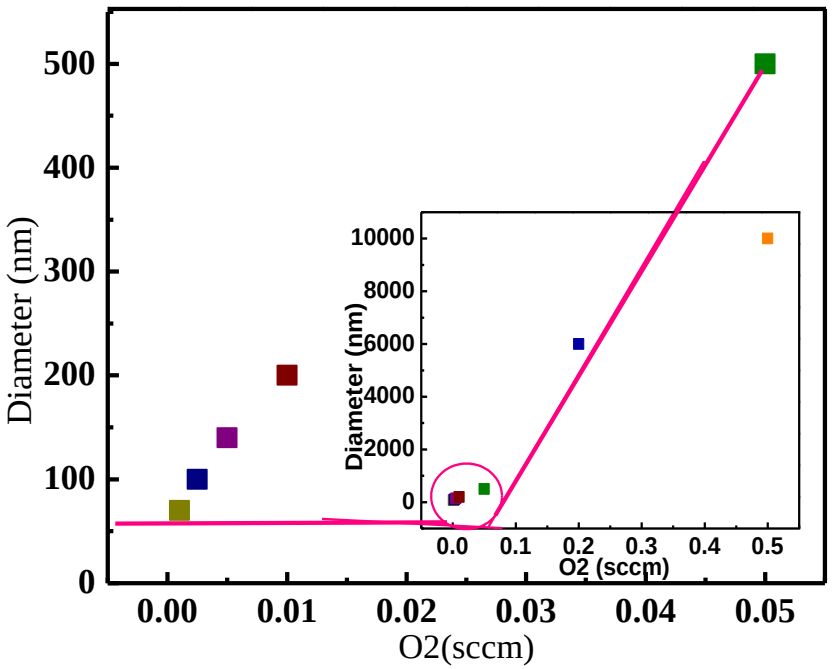

Figure 3. Nanorod diameter variation with oxygen flow rate over P-ECD seeded substrates.

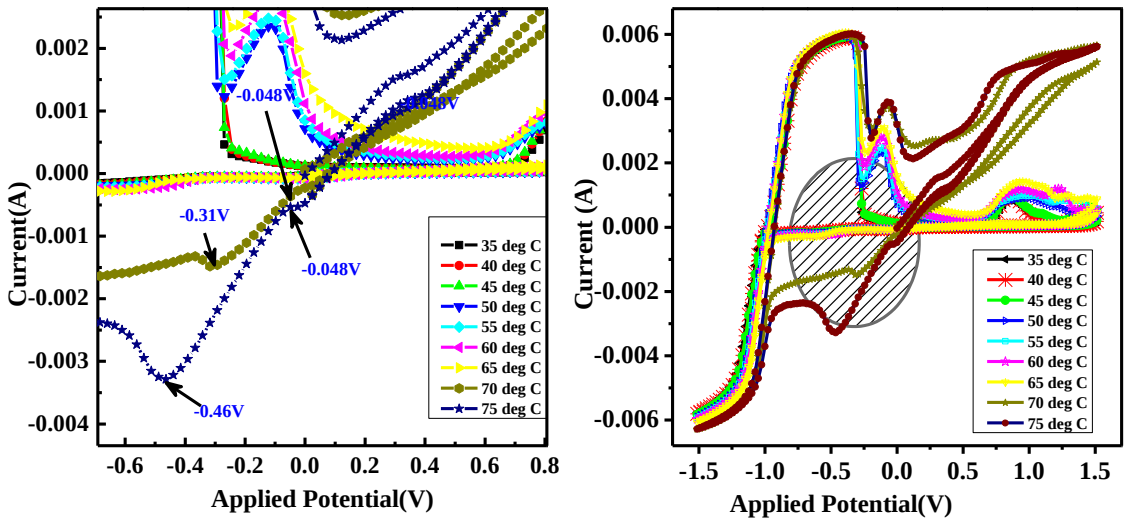

Figure 4. (a) Voltammogram for different temperatures and the ZnOH and ZnO forming cathodic peaks, (b) magnified peaks at 70^{o}C.

In the electrode the electrons are back scattered at the interface of the metal oxide layer and the TCO during the charge transportation and gives the dark current. This leakage current is one of the factors which reduce the efficiency in a device structure. The leakage current can be reduced with a compaction layer which acts as a fastener at the interface. In the present electrode the compaction layer and the seed layer are mended together for both verticality of the nanorods and reduction of electron backscattering.

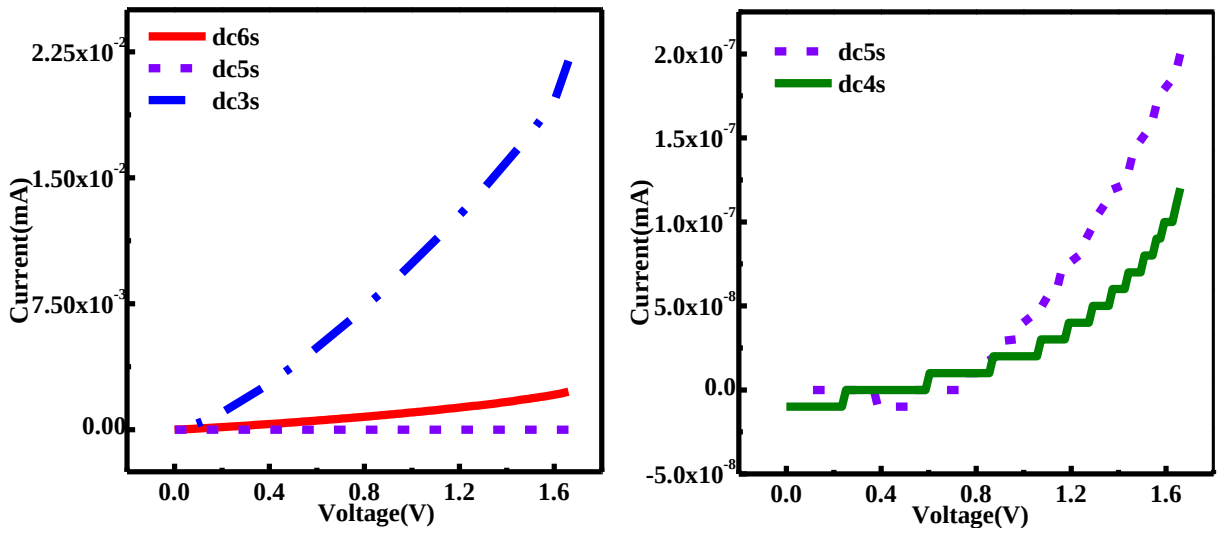

Figure 5. (a) Lowest dark current achieved for 100nm (5s) seed layer anode (b) Dark current Measurements of 100 nm (5s) and 80 nm (4s).

As the thickness plays a major role in the compaction layer in the reduction of dark current multiple layer seeds are prepared (40 nm, 60 nm, 80 nm, 100 nm, and 120nm). The samples are coded with the difference in layer thickness. For a pulse deposition of 100 seconds give the layer thickness of 20 nm. So the seed samples are coded as - 1s for 20 nm, 2s for 40 nm, and so on. The dark current is measured in Keithley meter with Lab view interface. The 100 nm (5s in figure 5) seed shows the lowest dark current (10^{-7}A) compared to the other multilayer seeded electrode as seen in figure (5). This low dark current is due to the low electron back scattering at the high crystalline state of the charge transporting layer. Seed layer thickness is the critical parameter that decides rod diameter and orientation of the nanorods [24, 25].

Defect reduction: Hundred nanometer seed layers are grown over FTO. The samples are then annealed in the Oxygen, Nitrogen and air stream at 130 ^{o}C for 20 minutes to reduce the surface defects. Samples with nanorods grown over annealed and un-annealed seed layers are prepared. After nanorod formation samples are again annealed at same annealing conditions of the seed layer and compared the performance with un-annealed samples. The samples used for the Mott Schottky (MS) analysis are n AS-R – non Annealed Seed and Rod layers, SAA-R – Seed Air Annealed and Rod non annealed, SNA-R – Seed Nitrogen Annealed and Rod non annealed, SOA-R – Seed Oxygen Annealed, SAA-RAA – Seed Air Annealed and Rod Air Annealed, SOA-ROA – Seed Oxygen Annealed and Rod

Oxygen Annealed, SNA-RNA Seed Nitrogen Annealed and Rod Nitrogen Annealed. These codes are used throughout the article refers to the above details of the sample preparation conditions.

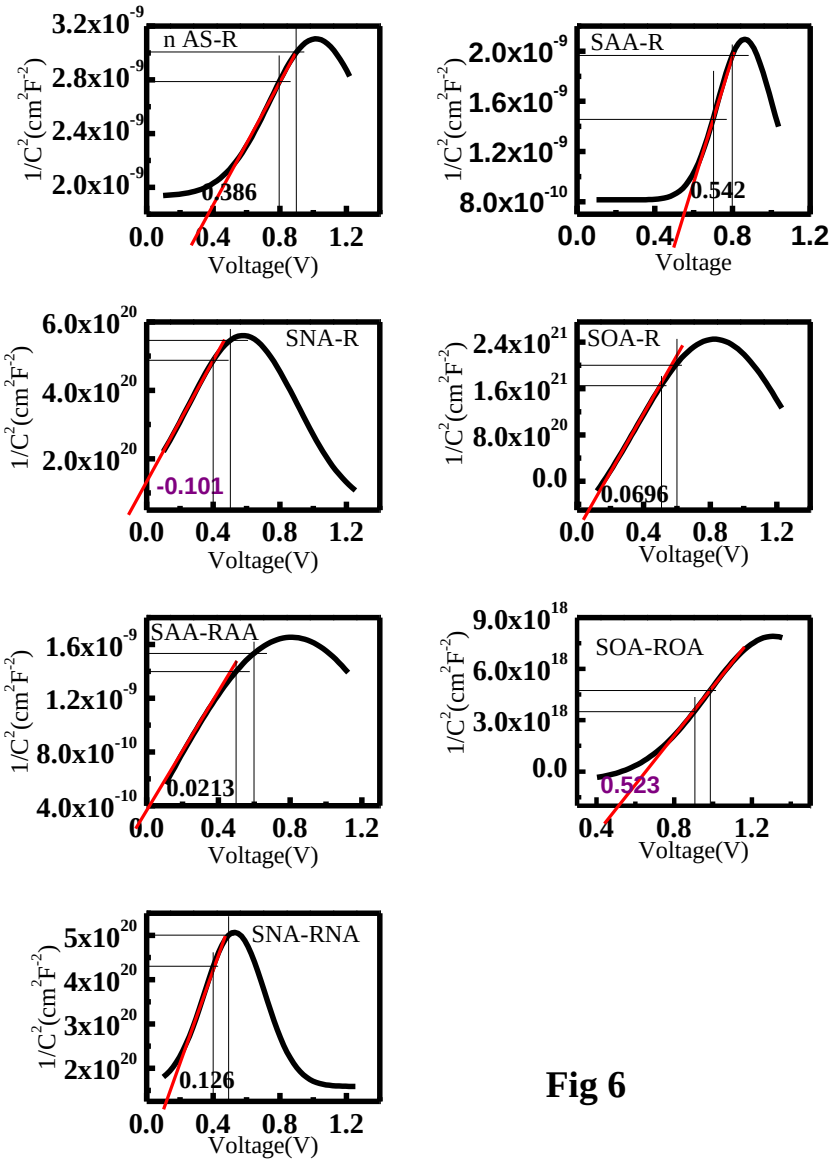

Fig 6

Figure 6. Mott Schottky plots for the samples n AS-R, SAA-R, SNA-R, SOA-R, SAA- RAA, SOA - ROA, SNA - RNA.

For charge density calculation, Mott Schottky (MS) analysis is carried out with Electrochemical Impedance spectroscopy (EIS). In two electrode system ZnO array is used as electrode and Pt mesh is used as the counter electrode. 0.1 M $LiClO_4$ in carbonate propylene is used as the electrolyte to avoid the decomposition of ZnO. EIS spectra are recorded in the frequency range of 100 MHz to 100 KH. The Mott Schottky plots and the Nyquist plots are prepared and analyzed based on the following equation,

$$\frac{1}{C^2} = 2/((e\varepsilon_0\varepsilon_r N_D A^2)) \left(V - V_{FB} - \frac{Kt}{e}\right)$$

Where ε_r= 10 is the dielectric constant of ZnO, and the $\varepsilon_0 = 8.85 \times 10^{-14}$ F/cm^2 and *e* is the positive electronic charge [26]. N_D is the charge density and VFB is the flat band potential and are calculated from the MS plot slope and intercept figure (6) from the following equations

$$N_D = \frac{2}{e\varepsilon_0\varepsilon_r A^2 (Slope)}$$

and

$$V_{FB} = -[\frac{intercept}{slope} + \frac{kT}{e}]$$

The MS plots show deviation from the straight line due to the porous nature of the nanorod electrode. Charge density values are tabulated in Table (2). The low N_D values in the Nitrogen and oxygen annealed implies reduction of the surface defect states at the interface. The air annealed and the non annealed samples have similar N_D values. In Oxygen annealing the Oxygen vacancies are filled so there is a reduction of defects. In the Nitrogen annealed samples as there is no available oxygen to fill the vacancy but the lattice adjustments repositions the Zn_i defects so there is a reduction in vacancy. So on both cases there is a defect reduction at the surface so there is a charge density reduction at the surface. This is further confirmed with PL analysis.

Table 2: charge density and flat band potential of samples.

Sl no	Sample	N_D – charge density(cm^2)	V_{FB}-Flat band potential(V)
1.	n A S-R	3.148×10^{21}	0.386
2.	SAA-R	2.50×10^{21}	0.542
3.	SAA-RAA	1.602×10^{21}	0.021
4.	SOA-R	9.36×10^{8}	0.069
5.	SOA-ROA	3.526×10^{10}	0.523
6.	SNA-R	1.499×10^{9}	-0.101
7.	SNA-RNA	5.762×10^{11}	0.126

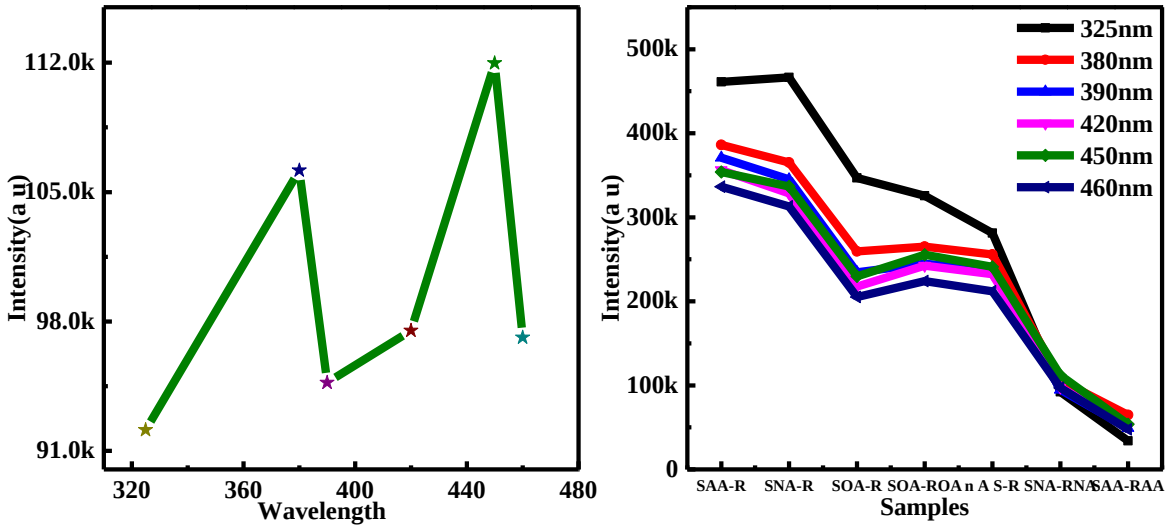

Figure 7. PL spectra with Gaussian fit of the Defect emissions at the Interfaces (i) n AS-R (ii) SAA-RAA (iii) SOA –ROA (iv) SNA-RNA

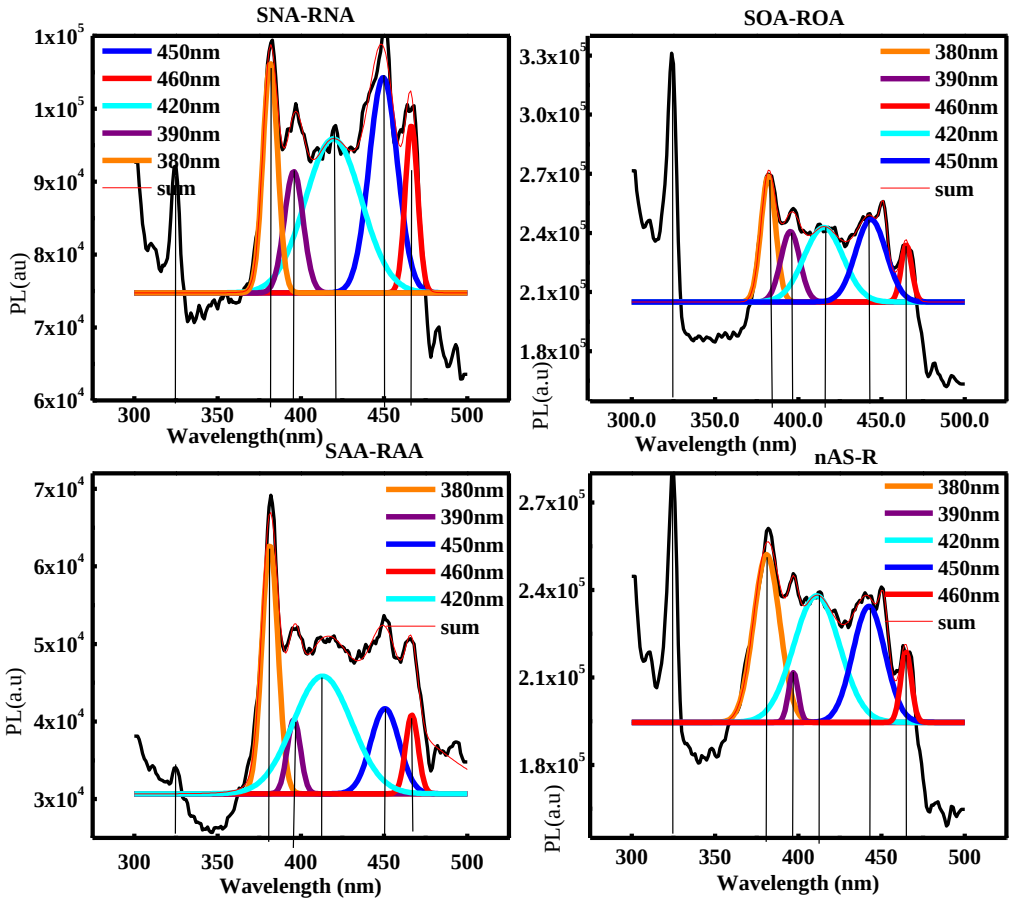

Figure 8. Comparative plot of the defect emission intensities of the samples and the Defect emissions of the Nitrogen annealed sample.

The surfaces and interfaces are the physical termination of the material, there exist more dangling bonds. This dangling bonds create mid band gap states which facilitates the radiative and non-radiative recombination. The photoluminescence of these surfaces states appreciably contribute when the charge density is low [27, 28].The prominent defect emissions in ZnO are at 380-500nm in the blue region is due to the Zn_i defects, at 480-600nm in the green region is of the V_o defects [29,30].

The PL spectra are made at room temperature with the excitation wavelength of 280nm.The Gaussian fit of the PL spectra show a clear exposition of the defect densities (figure7). As O_v is a shallow donor and the reduction of this defect is insignificant.

The PL study is focused on the reduction of defect mainly the Zn_i as it is the prominent electron trap which contributes the recombination during the charge transfer (at interfaces) and transport. The 325nm band edge emission (BEE) of ZnO and the intensities of the defect emissions are compared in the different samples annealed at different atmospheres. The air annealed sample has the higher emission peak at 380 nm and400 nm which is contributed by Zn_i defect. In the oxygen annealed samples the BEE emission is more as there is no reduction of defects. In figure (8) the Nitrogen annealed samples show a batho-chromic shift of the emission from 450 nm to 470nm which confirms the reduction of Zn_i defects [31]. The comparison of the defect emission peaks shows substantial reduction in the defects in Nitrogen annealed samples. BEE and the specific defect frequency emission intensities of the Nitrogen annealed sample are shown in the figure (8).

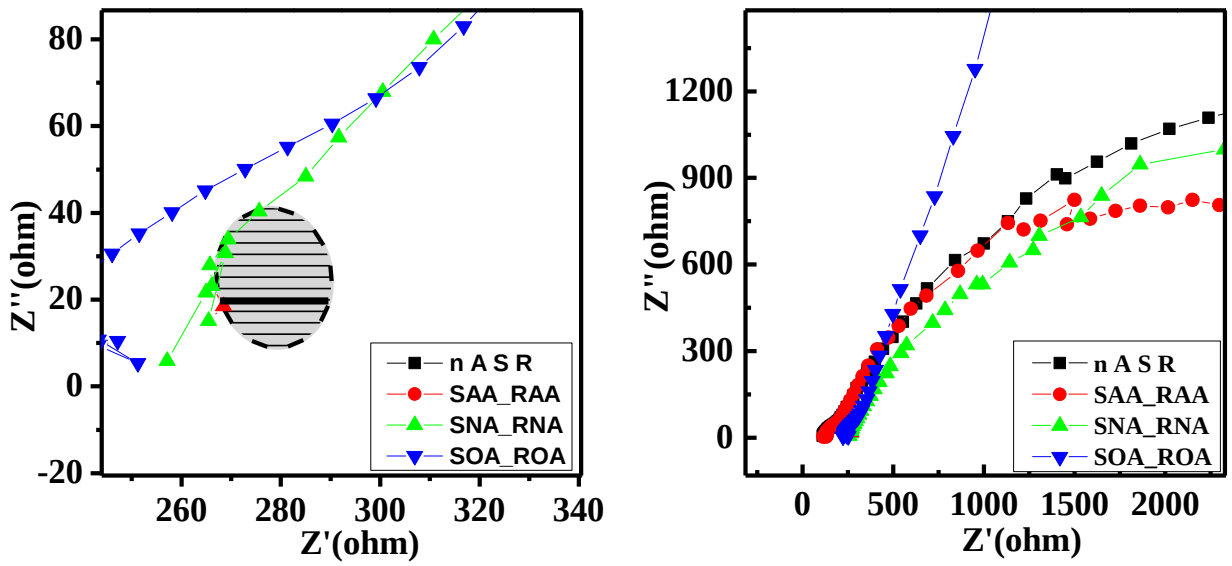

Figure 9. Nyquist Plot of the Samples – the small curvature of the Nitrogen annealed sample shows the lowest charge transfer resistance and impedance.

The impedance of the electrode is studied with the Nyquist plot in figure (9).The small semicircle at the high frequency region is the charge transfer at the interface. The elongated curved semicircle is due to the diffusion of charges by mass transfer at the electrolyte. The straight lines at the

low frequency region exhibit the pure capacitive behavior [32]. The Charge transfer resistance can be directly found from the radius of curvature of the Nyquist plot semicircle. The X axis intercept of the semicircle gives the R_{ct} values of the different samples. From the figure (9), it is clearly seen that the Nitrogen annealed sample has the lowest curvature with the value of R_{ct}30 Ω with the X axis intercept measurement. Other samples have impedances more than 100 Ω except air annealed as in the table (3). The reduction of R_{ct} implies higher conductivity at the interface. Thus in the Nitrogen annealed sample the charge transfer at the interface is effective when compared to the rest. So there is an efficient charge transfer resistance with the optimized electrode.

Table 3. The Impedance values of the samples.

Sl no	Sample details	Impedance values
1.	n A S-R	140
2.	SAA-R	140
3.	SOA-R	120
4.	SNA-R	180
5.	SAA-RAA	80
6.	SOA-ROA	120
7.	SNA-RNA	30

4. CONCLUSION

In conclusion we developed a low temperature two step electrochemical nanofabrication technique that can fine tune the morphology of the ZnO nanorod array electrode. The interfacial properties are substantially improved with this growth technique. The impedance spectroscopic studies and photoluminescence studies are effectively utilized for quantitative analysis of the interfacial properties and defect modification. The electron back scattering is reduced to the lowest value of 10^{-7}A. In the post fabrication heat treatment studies show that Nitrogen atmosphere the interfacial charge transfer resistance is reduced more than four times from 140Ω to 30 Ω and the charge density reduced by half compared to un-annealed sample. A substantial reduction in the interfacial defect has been well established with PL studies.

ACKNOWLEDGEMENT
The authors are thankful to University Grants Commission-Department of Atomic Energy for financial support. We are also thankful to Central Instrumentation Facility (CIF), Pondicherry University for providing necessary support for Characterizations.

References

1. D.V. Talapin, J.S. Lee, M.V. Kovalenko and E.V. Shevchenko, *Chem.Rev*., 110, 389-458 (2009)
2. R. Ferrando, J. Jellinek and R.L. Johnston, *Chem. Rev.*, 108, 845-910 (2008)
3. Dae-Yong Son, Jeong-HyeokIm, Hui-Seon Kim and Nam-Gyu Park, *J. Phys.Chem. C*., 116, 16567-16573 (2014)
4. R. Raza, Q. Liu, J. Nisar, X. Wang, Y. Ma and B. Zhu, *Electrochem. Commun*., 13, 917-920 (2011)
5. S.K. Arya, S.Saha, J. E. Ramirez-Vick, V. Gupta, S. Bhansali and S. P. Singh, *Anal. Chim. Acta*., 737, 1-21, (2012)
6. M.J.S. Spencer, *Prog. Mater. Sci.*, 57, 437-486, (2012)
7. D. Kim, K.Y. Lee, M.K. Gupta, S. Majumder and Sang-Woo Kim, *Adv. Funct. Mater*., 24, 6949-6955, (2014)
8. Th. Aeugle, H. Bialas, K. Heneka and W. Pleyer, *Thin Solid Films*., 201, 293-304, (1991)
9. L.K. van Vugt, Sven Rühle, R. Prasanth, H.C. Gettitson, K. L. Kuipers and D.A.M. Vanmaekelbergh, *Phys. Rev. Lett*., **97**, 147401 (2006)
10. R. Prasanth, L.K.vanVugt, D.A.M. Vanmaekelbergh and H.C. Gerritsen, *Appl.Phys.Lett*., 88, 181501, (2006)
11. LK Van Vugt, S Rühle and D Vanmaekelbergh, *Nano lett*., 6 (12), 2707-2711
12. L. Wang, X. Zhang, S. Zhao, G. Zhou, Y. Zhou and J. Qi, *Appl. Phys. Lett*, 86, 024108 (2005)
13. K.L. Foo, U. Hashim, K. Muhammad and C. H. Voon, *Nanoscale Res. Lett*., 9, 429-432, (2014)
14. L. Schlur, A. Carton, P. Leveque, D. Guillon and G. Pourroy, J. *Phys. Chem. C*., 117, 2993-3001, (2013).
15. Magdalena Skompska and Kamila Zarebska, *Electrochim. Acta*., 127,467–488, (2014)
16. Th. Pauporte´and D. Lincot, *J. Electroanal. Chem.*, 517, 54–62,(2001)
17. Sylvia Sanchez, Claude Lévy-Clément and Valentina Ivanova, *J. Electrochem. Soc*., 159(12) D705-D712 (2012)
18. Raul Salazar, Claude Lévy-Clément, Valentina Ivanova, *Electrochim.Acta*., 78, 547– 556, (2012)
19. J. Elias, R. Tena-Zaera and C. Lévy-Clément, , *J. Electroanal. Chem*., 621 171–177, (2008)
20. J. Elias, R. Tena-Zaera and C. Lévy-Clément, *Thin Solid Films*, 515, 8553–8557, (2007)
21. Th. Pauporté, G. Bataille, L. Joulaud and F. J. Vermersch, *J. Phys.Chem*., C, (2010),114, 194
22. T. Voss, C. Bekeny, J. Gutowski, R. Tena-Zaera, J. Elias, C. Lévy-Clément, I. Mora-Seró and J. Bisquert, *J. Appl.Phys*.,106, 054304 (2009)
23. M. D. Reyes Tolosa, J. Orozco-Messana, A. N. C. Lima, R. Camaratta, M. Pascual, andM. A. Hernandez-Fenollosa, *J.Electrochem. Soc.*, 158 (11) E107-E110 (2011)
24. Jia-Ling Wu, Han-Yu Lin, Yu-Cheng Chen, Sheng-Yuan Chu, Chia-Chiang Chang,Chin-JyiWu and Yung-Der, *ECS J. Solid State Sci. Technol.*, 2 (4) P115-P119 (2013)
25. Kyung Ho Kim, Kazuomi Utashiro, Yoshio Abe, and Midori Kawamura, *Int. J. Electrochem. Sci.*, 9 (2014)2080 – 2089
26. Iván Mora-Seró, Francisco Fabregat-Santiago, Benjamin Denier, Juan Bisquert, Ramón Tena-Zaera, Jamil Elias, and Claude Lévy-Clément , *Appl.Phys. Lett*.,89, 203117-19 (2006).
27. Dae-Hee Kim, Ga-WonLee and Yeong-Cheol Kim, *Solid State Commun*., 152, 1711-1794 (*2012*)
28. K. Gelderman, L. Lee, and S. W. Donne. *J. Chem. Educ*., 84 (2007)

29. Pipat Ruankham, Takashi Sagawa, Hiroshi Sakaguchi and Susumu Yoshikawa. *J. Mater. Chem*., 21, 9710 (2011)
30. David Charles Gleason-Rohrer, Bruce S. Brunschwig, and Nathan S. Lewis, *J. Phys. Chem. C, 117* , 18031–18042, (2013)
31. Sefaattin Tonga, JoonkiSuh, Can Ataca, Wen Fan, Alexander Luce, JeongSeuk Kang, Jonathan Liu, ChanghyunKo, Rajamani Raghunathanan, Jian Zhou, Frank Ogletree, Jingbo Li, Jeffrey C. Grossman and Junqiao Wu, *Sci. Rep.*, 3, 2657 (2013)
32. Zanhui Liu, Haihui Zhou, Zhongyuan Huang, Wenyang Wang, Fanyan Zengab and YafeiKuang,. *J. Mater. Chem. A*., 1, 3454 (2013)